JET-P(93)86

Heat Transport with Strong On and Off-Axis Heating

B Balet, J G Cordey.

JET Joint Undertaking, Abingdon, Oxon, OX14 3EA, UK.

Preprint of a paper to be submitted for publication in
Nuclear Fusion

October 1993

I. INTRODUCTION

A series of further experiments was undertaken on JET in 1992 to investigate if the transport of heat in a tokamak is local and diffusive. These experiments consisted of applying minority Ion Cyclotron Resonance Heating (ICRH) to similar 3 MA, 2.2 T L-mode discharges in which the resonance was located on-axis and 0.5 m off-axis. Combined on-and off-axis experiments were also undertaken. Two different types of discharge were used, the first one was a conventional edge fuelled discharge and in the second type the discharge was pellet fuelled prior to the onset of the heating. The purpose of the pellet fuelling was to provide a large central heat sink such that there was a significant region in which the heat flux is inward (i.e. negative).

Initial comparisons of on-and off-axis ICRH in the absence of pellet injection were completed in 1986 and reported in Callen et al [1]. These initial experiments which were at low ICRH power (≤ 5 MW) showed clearly that the change in the electron temperature profile depended on the location of the heating, however the ohmic heating (~ 2 MW) still had a significant effect in the power balance in the plasma centre with the off-axis case. In experiments reported in the present paper ICRH power levels in excess of 10 MW were used and the effect on the electron temperature profile of the position of the heating was much more significant.

The heating experiments following pellet injection described by Balet et al. [2] were also repeated at higher power levels. The basic conclusions of the previous reports [3,4] that the transport is local and diffusive was confirmed. However the increased data set means that more precise statements can be made concerning the modelling of the data with different forms for the heat flux.

The paper is divided into five Sections, in Section II the experimental data is described, in Section III the analysis of the results are presented and in Section IV possible model forms for the heat flux are discussed. Finally a summary is given in Section V.

II. DESCRIPTION OF THE DATA

The basic plasma was a standard 3.3 MA, 2.8 T limiter L-mode discharge. This was heated by hydrogen minority Ion Cyclotron Resonance Heating. Two different frequencies were used: the 42.6 MHz frequency was approximately on-axis whilst the 37.5 MHz frequency was some 50 cm off-axis, that is approximately midway between the

plasma centre and edge. Power levels up to 11 MW were available at each of these frequencies; the two frequencies could also be used together (mixed heating cases).

The time development of the main plasma parameters are shown in Fig. 1a for the on/off-axis heating cases with gas fuelling. The main difference between the off-and on-axis heated cases is seen in the responses of the central electron temperature, which increases more rapidly and reaches a much higher value with on-axis than off-axis heating. The total thermal stored energy is only marginally larger with on-axis heating than with off-axis heating since this quantity is strongly weighted in the outer region where the temperature profiles are very similar (see Fig. 2a). The sawtooth behaviour is also very different with the two types of heating, with off-axis heating the sawteeth are very small starting some six seconds after the start of the heating whilst in the on-axis heating case the sawteeth are larger and start slightly earlier (approximately five seconds from the start of the heating). The analysis is completed entirely in the sawtooth free period of Fig. 1a for both pulses.

In both these discharges the heat flux Q is always outwards even with off-axis heating since there is always sufficient central ohmic heating to overcome the central thermal inertia term. To achieve an inward heat flux with off-axis heating it is essential to introduce a large heat sink in the plasma centre and this is achieved by injecting a pellet immediately prior to the application of the heating. The large heat sink ensures a significant inward heat flux and a hollow temperature profile having a positive temperature gradient over the inner region. In this type of pulse it is possible to follow the evolution of heat flux from being inward to outward as the centre of the plasma heats up (see Fig. 3a).

A comparison of the development of the main plasma parameters for on-and off-axis heating following pellet injection is shown in Fig. 1b. Once again there is a marked difference in the time evolution of the central temperature whilst the total stored thermal energies are very similar in magnitude since the temperature values in the outer region are similar as can be seen from Fig. 3a.

The sawtooth behaviour is very different in the two pulses, with on-axis heating the sawteeth are large and start one second after the commencement of the heating whilst with off axis heating there are no sawteeth throughout the whole heating phase.

Finally in Fig. 4, the development with time of a mixed heating case is shown following pellet injection. For the first second of the heating phase 6 MW of off-axis

heating was used and then a further 4 MW of on-axis heating was added. Note the strong response of the central electron temperature following the switch-on of the on-axis heating and the subsequent appearance of large sawteeth.

Thus to summarise this section, it appears that in all the different types of pulses the temperature profile responds to the location of the source of heating, having a hollow or flat central temperature with off-axis heating and a strongly peaked temperature with on-axis heating.

III. DATA ANALYSIS AND THE POWER BALANCE

A complete transport analysis of all of the above pulses has been made using the TRANSP code [5]. Both the ICRH model in TRANSP [6, 7] and the PION model [8] have been used, the two models are found to give very similar heating profiles, examples are given in Figures 2b and 3b. The bulk of the background plasma heating comes from the energetic hydrogen minority ions, there is however a small contribution (< 10%) from transit time magnetic pumping in addition to the ohmic input which is also small (< 10% of total heat input).

The ion temperature profile was not measured in these pulses. However, the peak ion temperature measured by the X-ray Crystal spectrometer closely followed the central electron temperature [2], and $T_i = T_e$ is therefore assumed in the analysis of these pulses.

Several consistency checks of the data were done using the TRANSP code. The most important result being that the kinetic measurements reproduced the total stored energy measured by the diamagnetic loop. Two examples of such a consistency check are shown in Figs. 5a and 5b for the on-and off-axis pulses without pellet injection. The fact that the simulated diamagnetic measurement from the TRANSP code reproduces well the actual measurement confirms that both the kinetic measurements and the calculation of the minority fast ion energy within the code are reasonably accurate. Consistency checks between the measured and simulated loop volts and neutron emission rates further confirmed the validity of the input measurements used by TRANSP i.e. the Zeff from Visible Bremsstrahlung and of the assumption made in the analysis of all these pulses that $T_i = T_e$.

A further key consistency check upon the calculated power deposition profile is to compare it with the initial rate of change of the stored energy profile. This is done in

Fig. 6a and 6b for the on-and off-axis without pellet injection, at a time some 0.1s from the start of the heating. The curves have been normalised to the calculated electron heating profile in both cases to show that the electron heating profile and the response are in good agreement. The normalisation factor however was close to unity in both cases.

Turning now to the power balance, this consists of five significant terms, the ICRH (P_{ICRH}) and ohmic (P_{OH}) input terms, the thermal inertia ($\dot{W}$) and the radiation (P_{rad}) loss terms, and the conductive heat flux (the convective heat flux is very small). The high density of these pulses, $n_e(o) > 6 \times 10^{19}$ m^{-3} in the pulses in which pellets were injected and $n_e(o) > 4 \times 10^{19}$ m^{-3} in the non pellet pulses, means that it is not possible to separate the ion and electron channels and as mentioned earlier there are no ion temperature profile measurements in these pulses. The equation for the total (ion + electron) conducted heat flux Q has the form

$$Q.S = \int_0^\rho P_{ICRH} + \int_0^\rho P_{OH} - \int_0^\rho \dot{W} - \int_0^\rho P_{rad} \qquad (1)$$

where S is the surface area of the flux surface ρ (ρ is the horizontal width of each magnetic surface normalized to the width of the outer magnetic surface).

When the heating is switched on the main balance is between the ICRH term, the thermal inertia term and the heat flux term. With on-axis heating the heat flux Q is always positive (i.e. outward), however with off-axis heating provided the thermal inertia in the plasma centre is large enough the heat flux initially is inward in the central region and then as the plasma centre heats up the thermal inertia term becomes smaller and the heat flux becomes outward. Coincident with the change in sign of the heat flux in the central region the temperature gradient also changes sign [2], indicating that any heat pinch term must be small. This will become clearer in the next section where the scaling of the heat flux is discussed.

IV. SCALING OF THE HEAT FLUX

In Fig. 7 the total heat flux Q is shown versus - $n_e \nabla T_e$ for the on-axis, off-axis and mixed heating cases following pellet injection at several radial positions. The separate points show the time evolution from t = 4.0s just after the start of heating until t = 6.0s when a steady state is reached. For the on-axis and mixed heating pulses with pellets the region around the sawtooth was excluded. At each radius the group of points nearest the origin is from the off-axis heated pulse, the next group is the mixed heating case and

the final group the on-axis heated case. An important point to note is that for the inner radii ($\rho = 0.25$ and $\rho = 0.35$) the curves go very close to the origin indicating the absence of any heat pinch terms. The slopes of the curves also increase with radius indicating that the thermal diffusivity increases with radius, a common feature of all L-mode plasmas.

The data can be approximately put on a universal curve by multiplying the abscissa $- n_e \nabla T_e$ by $q_\psi^{1.75}$ where q_ψ is the local safety factor, this is shown in Fig. 8. There is no particular reason for choosing the safety factor q_ψ as the shear s or any other radially increasing parameter could have been used. It is clear from Fig. 8 that the heat flux is not linearly dependent on $q_\psi^{1.75}\, n_e \nabla T_e$, that is χ_{eff} must also increase with $|\nabla T_e|$ or T_e. This is the local equivalent of the degradation of the global confinement time with power. Now in practice one can model the data of Fig. 8 in several different ways and a few examples are given in Figs. 9a, b, and c. Firstly the data is modelled by a critical gradient form $Q = \chi n_e(\nabla T_e - \nabla T_c)$ where χ is independent of ∇T_e. This is similar to the model used by Rebut, Lallia, Watkins [9]. In Figs. 9b and 9c a quadratic and a cubic form in ∇T_e are shown. Clearly all of the above forms give a reasonable representation of the data. There are other possibilities as well since the temperature itself also varies with ∇T_e. Since the range of variation is very small (3 to 4 keV for the $\rho = 0.25$ case) a very strong dependence on temperature, at least cubic is needed. This would give a degradation with power of $P^{-0.75}$ which is somewhat higher than is observed.

The non pellet pulses have a similar Q versus $- n_e \nabla T_e$ evolution as the pellet cases but of course the range of variation in $- n_e \nabla T_e$ is much smaller and the temperature profile is never hollow with an inward heat flux. In Fig. 10 the steady state non-pellet data is compared with the "universal" curve of Fig. 9a for both on-and off-axis heated pulses. The non-pellet data lies within the errors bars of the line showing that the χ_{eff} profiles are similar.

V. SUMMARY

These comprehensive on/off ICRH experiments further reinforce the results of the earlier experiments namely that the electron temperature profile responds to the heating profile. By the injection of pellets into the centre of the plasma to create a large thermal sink, it has been possible to study both positive and negative regions of Q and $- n_e \nabla T_e$, no evidence of the existence of any substantial heat pinch in the total heat flux has been found. The total heat flow is always down the temperature gradient. The

complete data set, on/off axis heating with and without pellets, can be described by a relatively simple local diffusive model of the form,

$$Q = -\chi\left(q_\psi, |\nabla T_e|\right) n_e \nabla T_e \qquad (2)$$

where χ is proportional to $q_\psi^{1.75}$ and increases with $|\nabla T_e|$. The data is not good enough to determine conclusively the precise dependence of χ on $|\nabla T_e|$ and several forms were shown to give a reasonable fit.

ACKNOWLEDGEMENT

The authors gratefully acknowledge the production of the data in this report by their colleagues in the JET experimental team, in particular P. Lomas, T.T.C. Jones, D. Ward, H.W. Morsi and finally D.V. Bartlett for assistance with the ECE data. Pellet injection work in JET is performed under a collaboration agreement between JET and the United States Department of Energy.

REFERENCES

[1] Callen, J.D., Christiansen, J.P., Cordey, J.G., et al., Nucl. Fusion 27 (1987) 1857.

[2] Balet, B., Cordey, J.G., Muir, D.G., et al., Nucl. Fusion 32 (1992) 1261.

[3] The JET Team (presented by M. Keilhacker), 14th IAEA Conference on Plasma Physics and Controlled Nuclear Fusion Research, Würzburg (1992), IAEA-CN-56/A-1-1.

[4] The JET Team (presented by J.G. Cordey), 14th IAEA Conference on Plasma Physics and Controlled Nuclear Fusion Research, Würzburg (1992), IAEA-CN-56/D-3-4.

[5] Goldston, R.J., McCune, D.C., Towner, H.H., et al., J. Comput. Phys. 43 (1981) 61.

[6] Smithe, D.N., Colestock, P.L., Kashuba, R.J., et al., Nucl. Fusion 27 (1987) 1319.

[7] Hammett, G.W., Ph.D. Thesis, Princeton University (1986), available from University Microfilms, Ann Arbor MI 48106 (USA).

[8] Eriksson, L.G., Hellston, T. and Willen, U., Submitted to Nucl. Fusion.

[9] Rebut, P-H., Watkins, M.L., Gambier, D.J., et al., Phys. Fluids (B) 3 (1992) 2209.

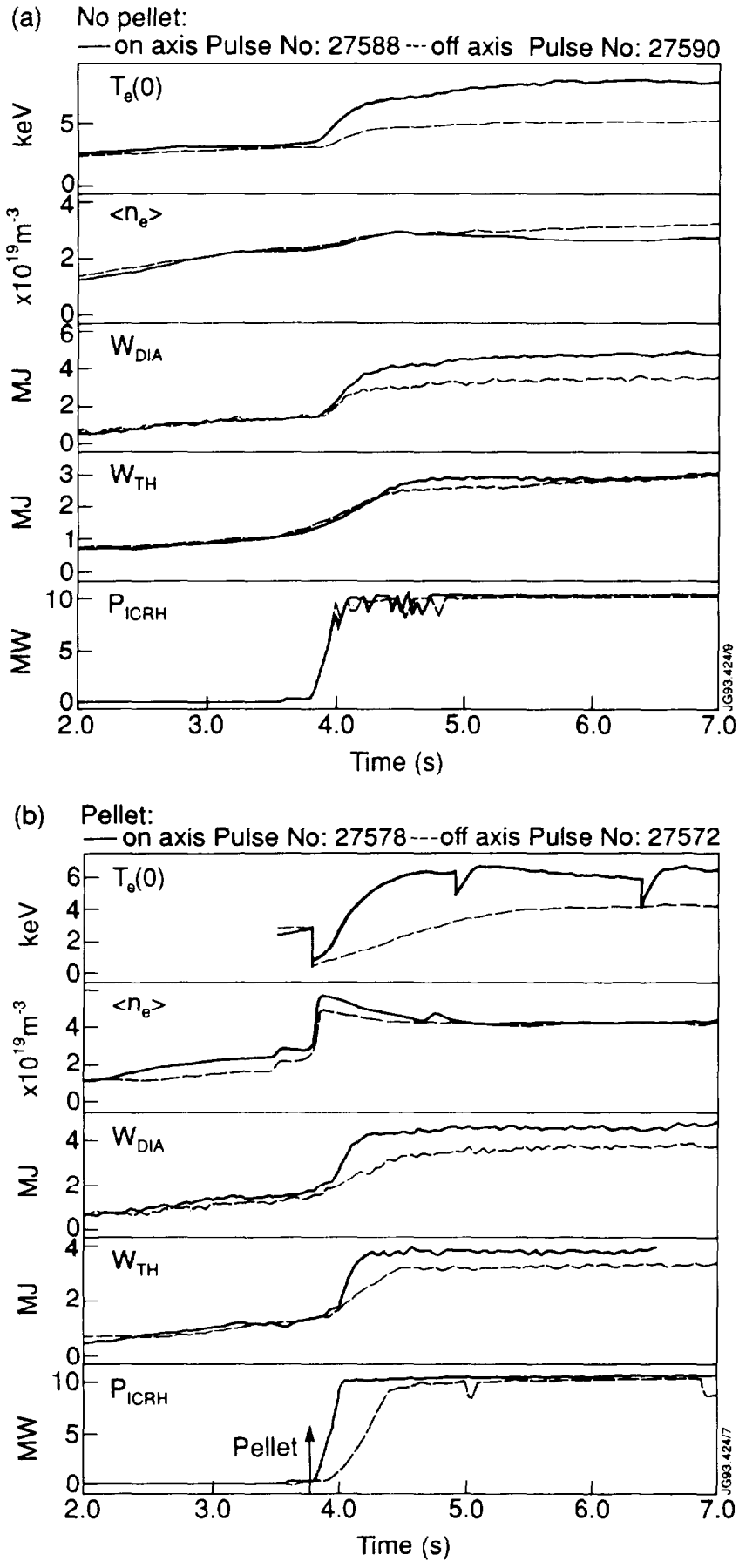

Fig. 1. The time evolution of the central electron temperature $T_e(o)$, the volume - averaged electron density $\langle n_e \rangle$, the plasma diamagnetic energy W_{DIA}, the thermal stored energy W_{TH} and the ICRH input power for on-axis (solid line) and off-axis (dotted line) heating in [a] two pulses with gas fuelling, [b] two pulses with pellet injection.

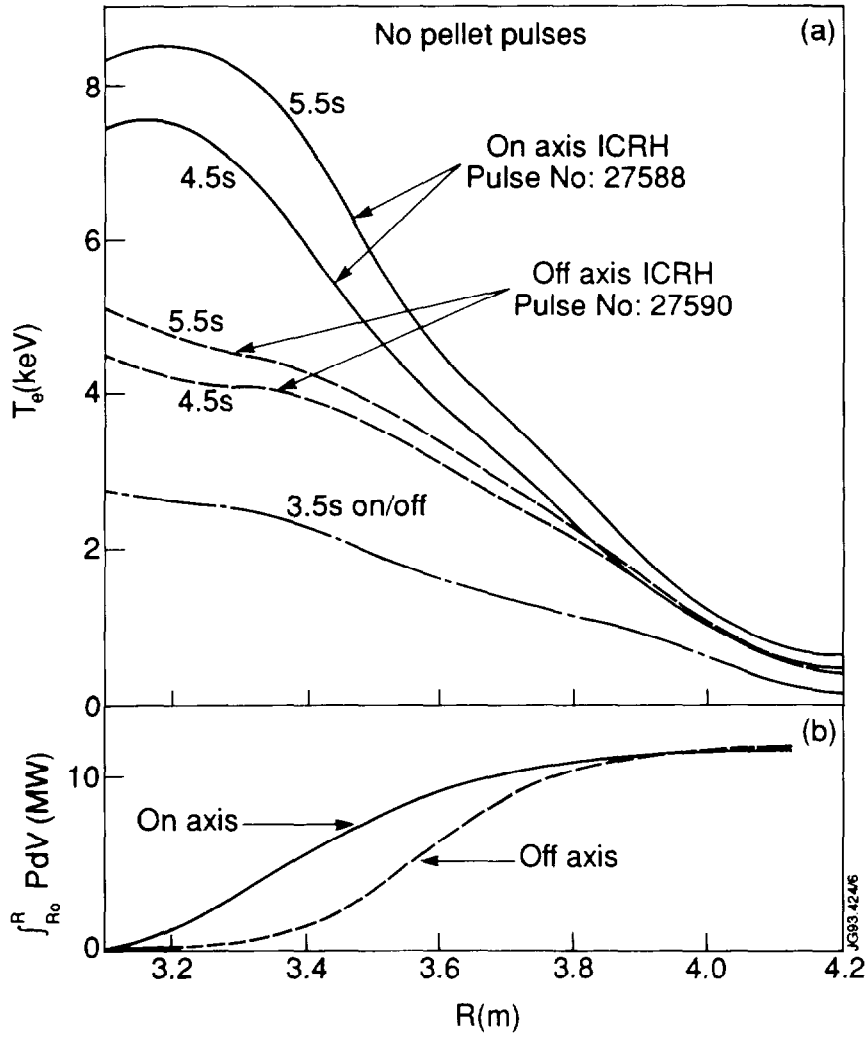

Fig. 2. [a] Radial electron temperature profile at different times for the on-axis (solid line) and off-axis (dotted line) heating cases with gas fuelling. [b] total volume integrated heating power (ICRH + ohmic) for both cases.

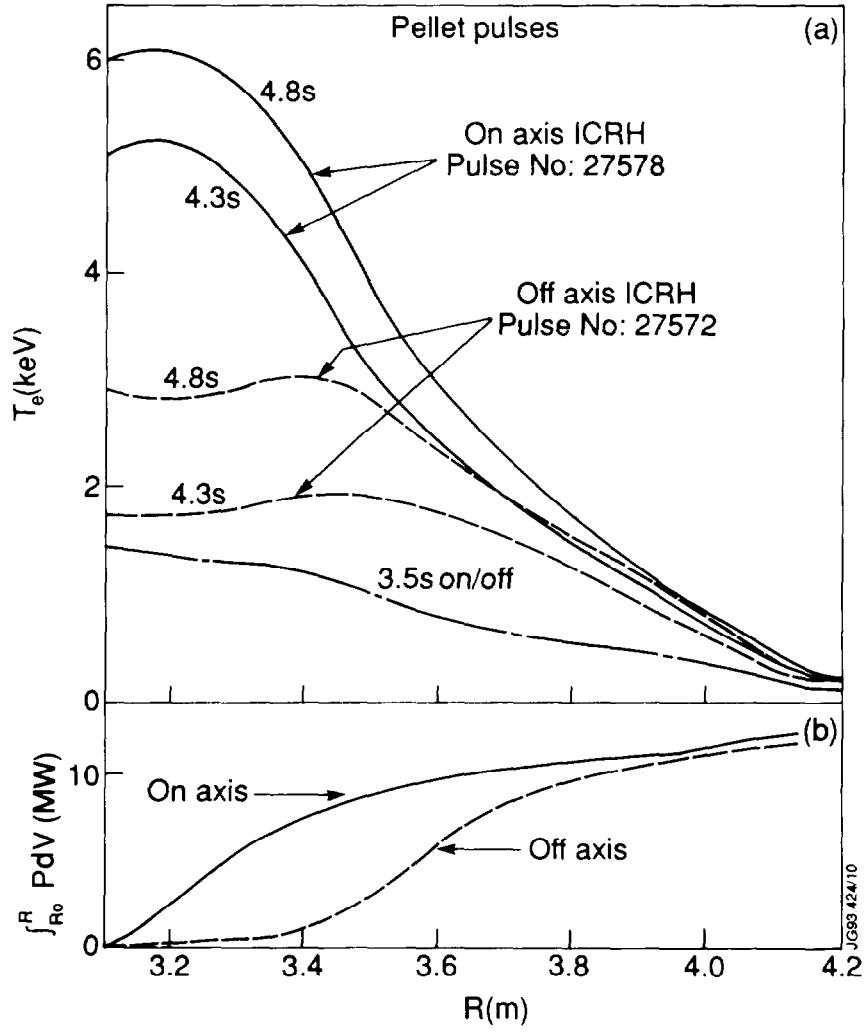

Fig. 3. a) Radial electron temperature profile at different times for the on-axis (solid line) and off-axis (dotted line) heating cases with pellet injection. b) total volume integrated heating power (ICRH + ohmic) for both cases.

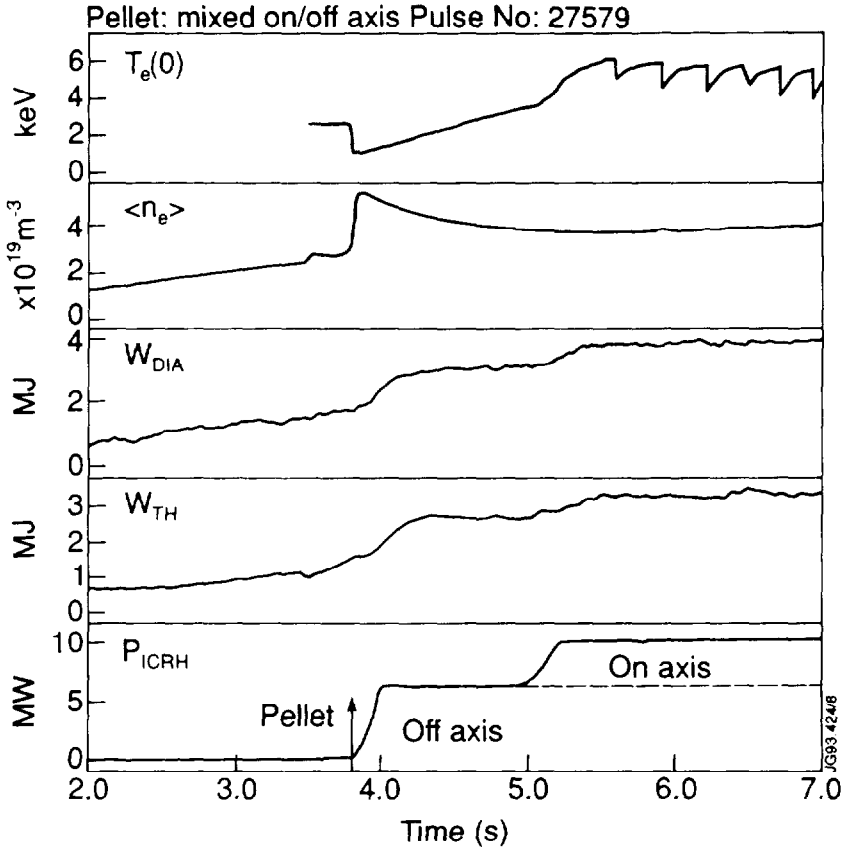

Fig. 4. The time evolution of the central electron temperature $T_e(o)$, the volume averaged electron density $<n_e>$, the plasma diamagnetic energy W_{DIA}, the thermal stored energy W_{TH} and the ICRH input power for a mixed heating case. The on-axis heating is switched on at t = 5s, one second after the off-axis heating.

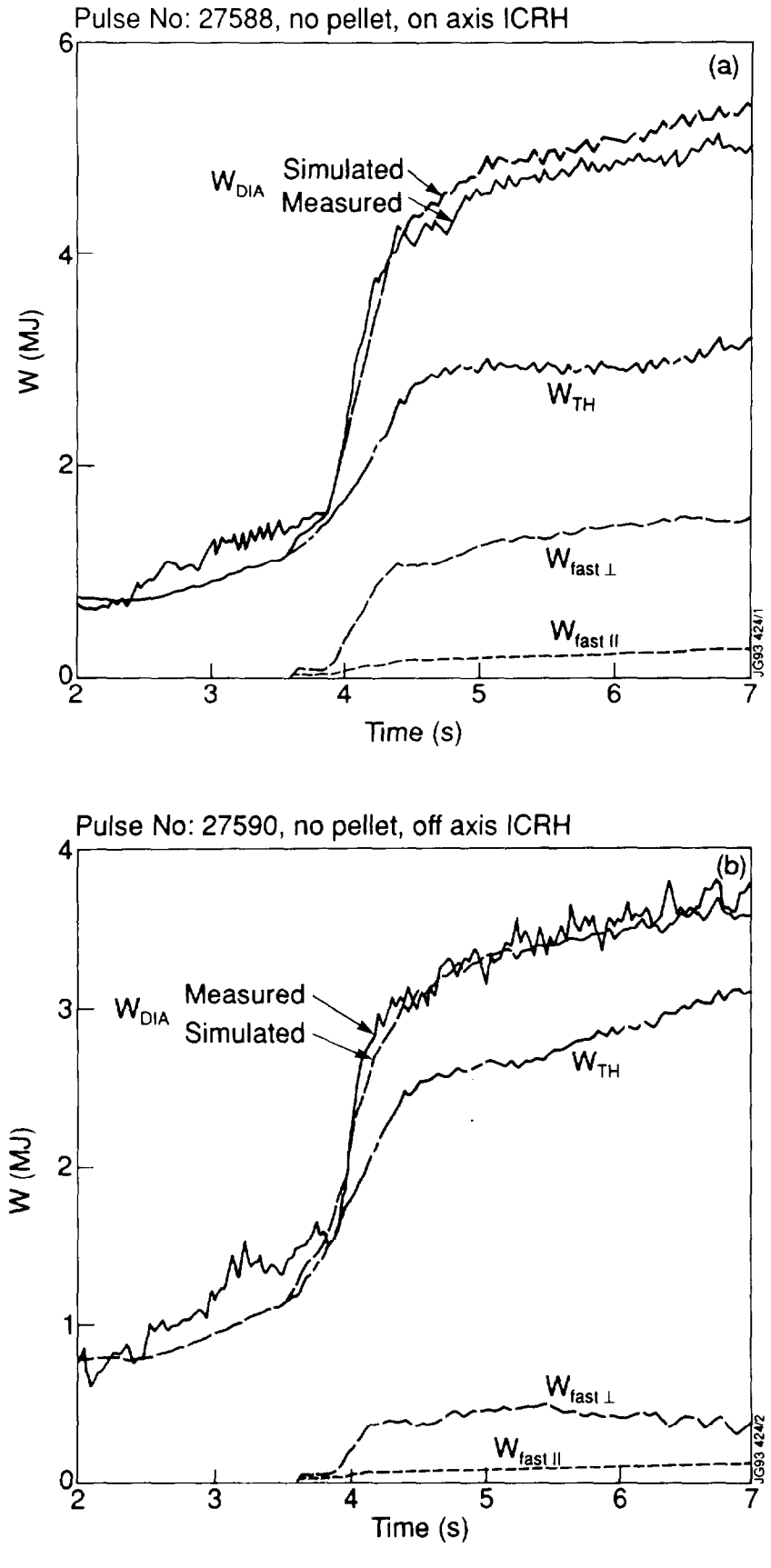

Fig. 5. The time evolution of the measured and simulated plasma diamagnetic energy W_{DIA} for [a] the on-axis and [b] the off-axis heating pulses without pellet injection. Also shown are the thermal stored energy W_{TH} and the fast ion contributions $W_{fast\perp}$ and $W_{fast||}$ computed by TRANSP.

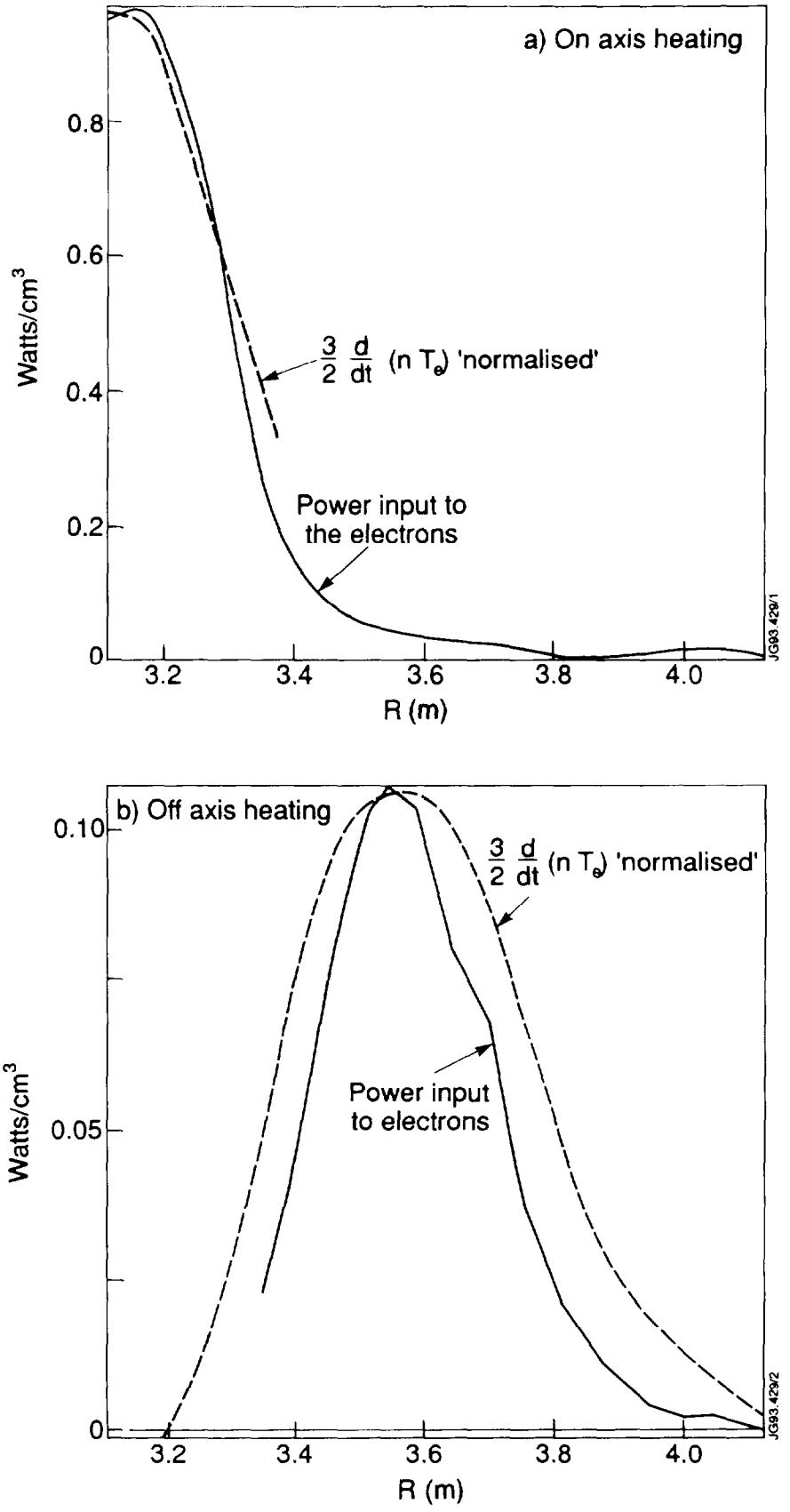

Fig. 6. Power transferred to the electrons from the ICRH for a) the on-axis and b) the off-axis heated pulses without pellet injection and the initial plasma response at 0.1s from the start of heating.

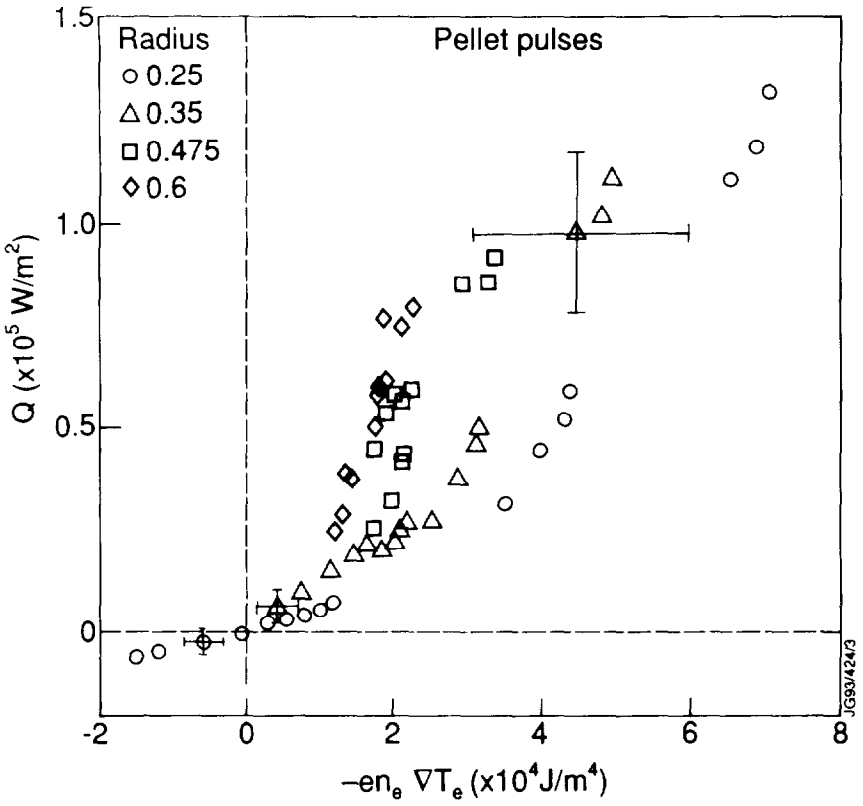

Fig. 7. The total heat flux Q defined by Eq. (1) versus - $en_e\nabla T_e$ at different values of the normalised radius ρ for the discharges with on-axis, off-axis and mixed heating following pellet injection.

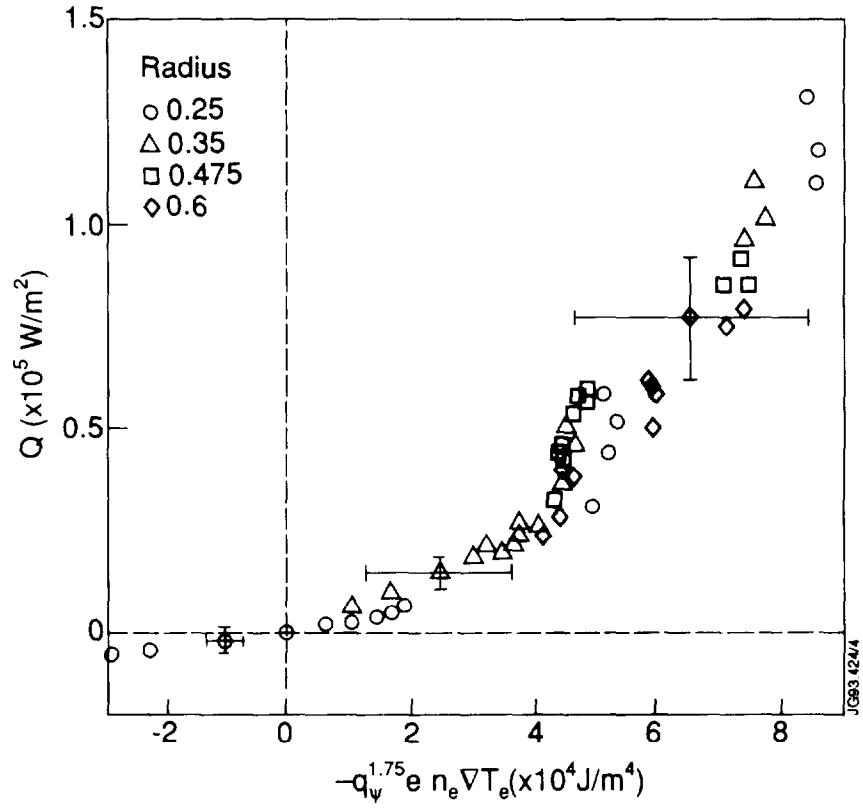

Fig. 8. The total heat flux Q defined by Eq. (1) versus - $q_\psi^{1.75} e\, n_e\nabla T_e$ at the same radii ρ and for the same discharges shown in Fig. 7.

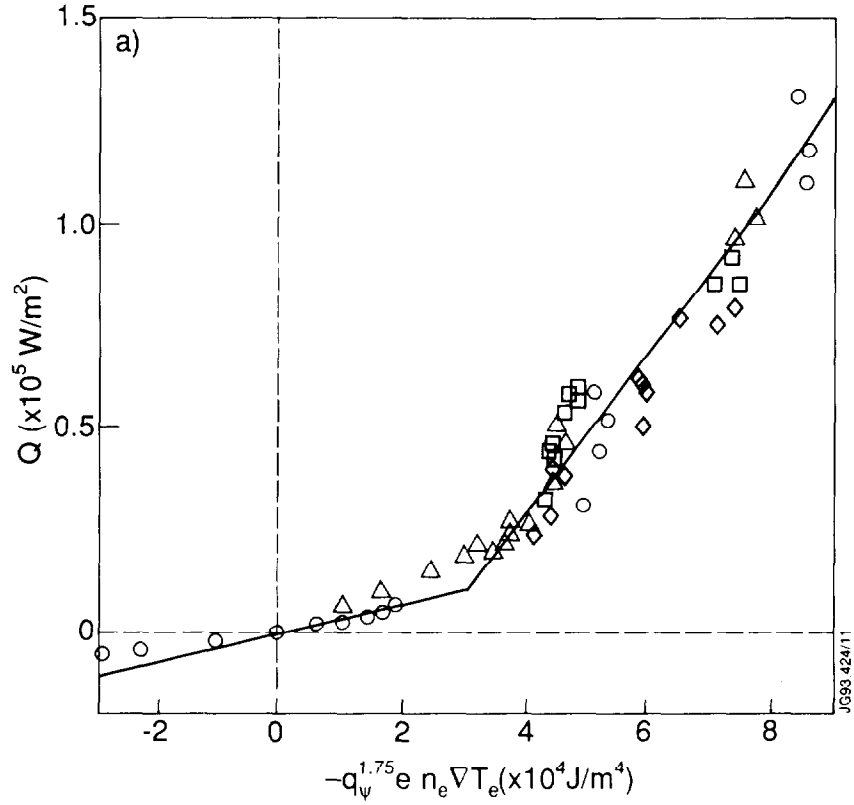
a)
1.5
1.0
0.5
0
Q (x10^5 W/m^2)
-2
0
2
4
6
8
-q_ψ^1.75 e n_e ∇T_e (x10^4 J/m^4)
JG93.424/11

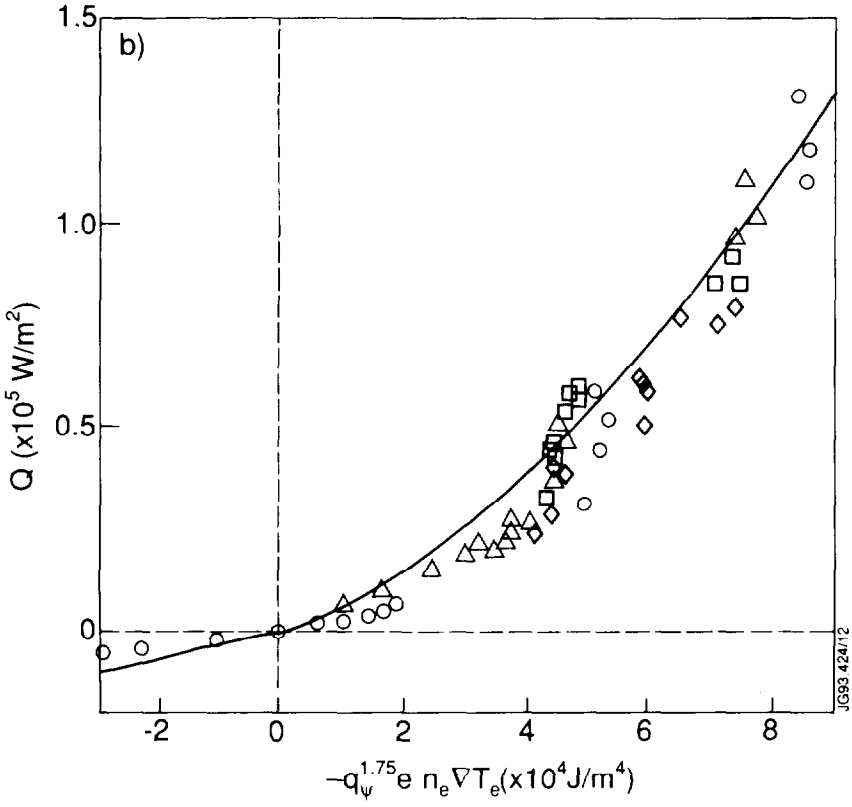
b)
1.5
1.0
0.5
0
Q (x10^5 W/m^2)
-2
0
2
4
6
8
-q_ψ^1.75 e n_e ∇T_e (x10^4 J/m^4)
JG93.424/12

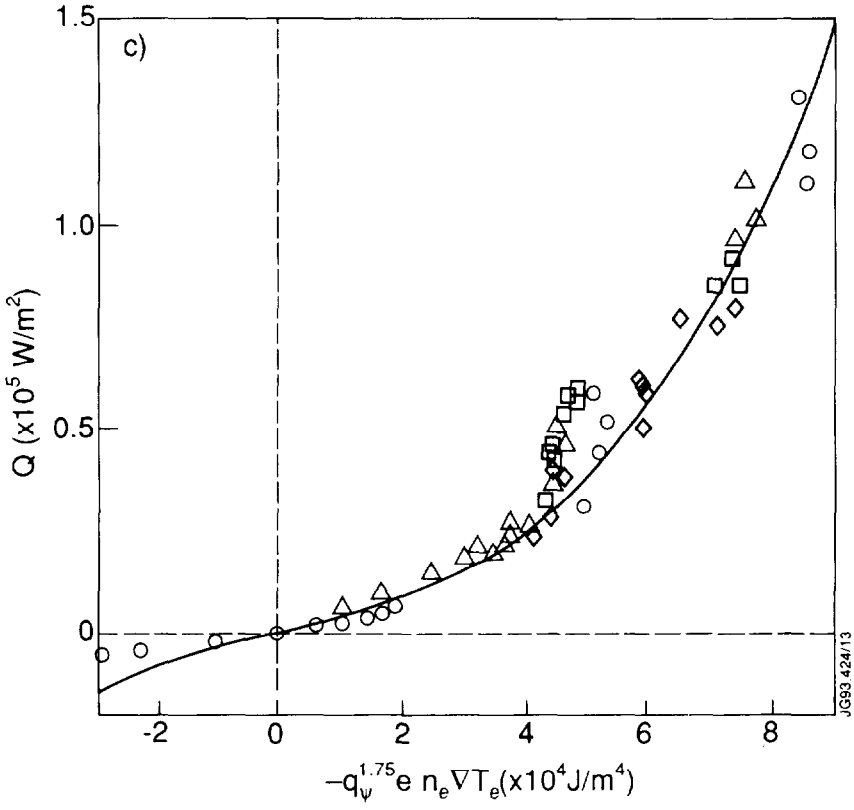

Fig. 9. Modelling of the data of Fig. 8 by [a] a critical gradient form $Q \simeq \chi n_e (\nabla T_e - \nabla T_c)$, [b] a quadratic form $Q = x\,(1.09\ 10^{-5} x + 0.5)$ and [c] a cubic form $Q = x\,(1.29\ 10^{-10} x^2 + 0.55)$ where $x = -\ q_\psi^{1.75} e\ n_e\ \nabla T_e$.

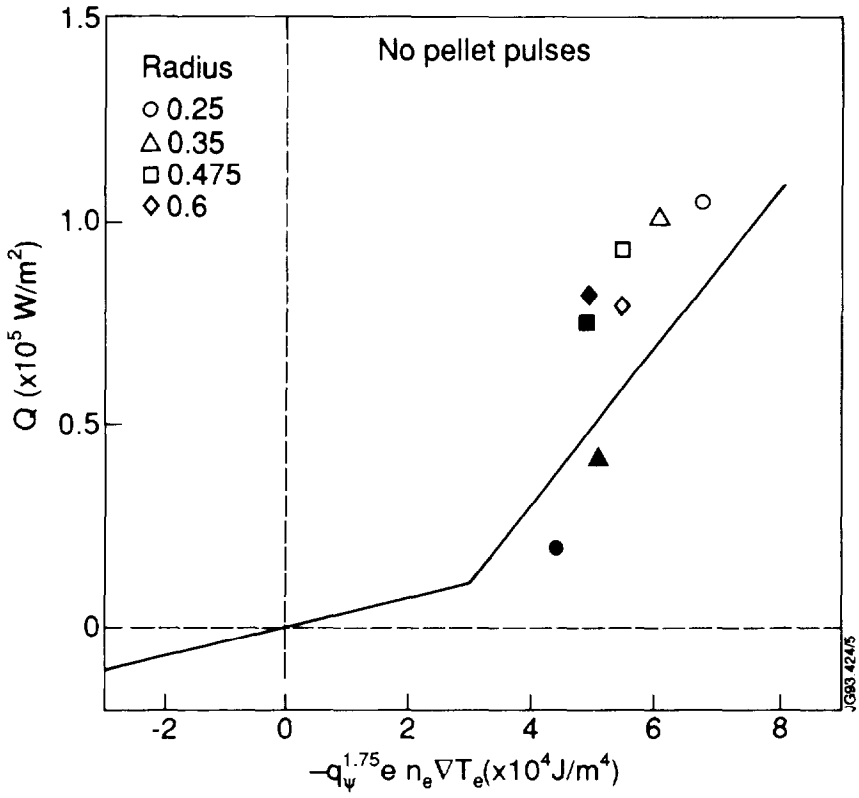

Fig. 10. The total heat flux Q defined by Eq. (1) versus - $q_\psi^{1.75} e\, n_e \nabla T_e$ at different values of the normalised radius ρ for the discharges without pellet injection. The solid curve is the critical gradient model fit of Fig. 9a. The solid symbols are for the off-axis heating case and the open symbols are for the on-axis heating case.